RICE UNIVERSITY

TEMPERATURE DEPENDENCE OF TIME RESOLVED $(ArXe)^{+}$ EMISSION

by

Louis M. Houston

A THESIS SUBMITTED
IN PARTIAL FULFILLMENT OF THE
REQUIREMENTS FOR THE DEGREE

MASTER OF ARTS

APPROVED, THESIS COMMITTEE:

G. K. Walters
Professor of Physics
Chairman

S. D. Baker
Professor of Physics

G. P. Glass
Associate Professor of Chemistry

HOUSTON, TEXAS
APRIL, 1983

TEMPERATURE DEPENDENCE OF TIME RESOLVED $(ArXe)^+$ EMISSION

by

Louis M. Houston

ABSTRACT

Rare gas binary mixtures under electron bombardment are characterized by strong emissions that have been traced to radiative transitions of diatomic heteronuclear ions (e.g.,$(ArXe)^+$).The kinetic processes governing heteronuclear ion formation and decay are not well understood,but the more important of these processes should be elucidated by time resolved spectroscopy. In particular, since heteronuclear rare gas ions are known to be only weakly bound, their characteristic emissions are expected to be greatly affected by changes in temperature. Under this assumption,an experiment was devised to study the $(ArXe)^+$ 328nm emission under time resolved conditions for different temperatures and mixtures of the gas. The experiment necessitated the design and installation of a temperature variable gas cell. Although the apparatus allows one to vary temperature over a wider range,data,thus far, were taken between 248K and 348K. In this range, preliminary time dependent spectra have been observed to vary significantly as a function of temperature.

ACKNOWLEDGEMENTS

The author is particularly indebted to Dr. G. K. Walters, who is always encouraging and instructive, making the work involved in this thesis considerably easier.

Thanks are extended to Mr. M. G. Durrett for continuing to guide and aid the author in the lab and for his collaboration in this work.

The author is grateful to Mr. D. B. Vanderslice for his helpful assistance in the lab.

Last, but not least, the author would like to express his eternal gratitude to his parents, whose love and understanding are an unending source of motivation.

TABLE OF CONTENTS

LIST OF FIGURES

INTRODUCTION

Over recent years there has been much interest in the molecular properties of electron beam excited heavy rare gases. This interest is largely due to the possibility of these gases forming high energy excimer lasers. An excimer can be loosely defined as a diatomic molecule whose ground state is unstable at room temperature. The ground level in an excimer laser is therefore dissociative and hence unpopulated. The result is an automatic population inversion of the laser transition. All rare gas diatomic molecules and ions are excimers and their lower excited states are found to be efficiently populated by electron impact [1]. One might therefore expect the resulting bound-free fluorescence to form a strong laser transition. Unfortunately, due to other processes, rare gas systems studied thus far have experimentally made inefficient lasers [2]. It is the understanding of these processes that motivates continued study of rare gas systems.

It has been found by several groups that in certain binary mixtures of the rare gases there are emission bands belonging to neither of the component gases but characteristic of the mixtures themselves. In fact Tanaka et al. [3] observed that nine of the ten binary mixtures of He, Ne, Ar, Kr and Xe, when excited in an electrical discharge, emitted one or several bands which are unique to the mixture. These emissions do not exist under like conditions for any of the pure rare gases. It was discovered that each of these bands peaked near a wavelength which corresponded to the energy difference between one of the atomic ion levels of the lighter rare gas atom and one of the atomic ion levels of the heavier rare gas atom. Similar bands had been seen earlier in Ar/Kr, Ar/Xe and Kr/Xe mixtures by Friedl [4] and Kugler [5] using

high energy electron beam excitation. Though these earlier experimentalists had attributed the bands to neutral heteronuclear molecule emissions,the bands they discovered were consistent with the suggestion of Tanaka et al., that they involved ion levels.

Consistent with reports by Forestier and Fontaine (1978) [6] and Millet et al. (1980) [7], an emission band at 328nm attributed to the $(ArXe)^+$ ion has been seen after electron bombardment. In order to study the kinetics of this molecular ion, time resolved spectroscopy was used. This involves monitoring the time dependence of bound-free fluorescence following a short burst of charged particles (e.g.,electrons). Using this method values for reaction rates can be obtained by curve fitting the time dependent spectrum.

The only other kinetic study of the $(ArXe)^+$ ion was done by Millet et al. This group experimented with Ar/Xe gas mixtures at room temperature. Their basic conclusion was that a two component kinetic process exists: $(ArXe)^+$ ions are "slowly" formed by three-body collisions and are "quickly" destroyed by radiative decay.

In this experiment, it was desired to gain more information on the Ar/Xe reaction rates by varying gas temperature. It is apparent that there should be significant temperature effects due to the weak binding in heteronuclear ions. This weak binding is evidenced in $(ArXe)^+$ by the small difference between the 328nm emission seen and the 325nm limiting wavelength for charge-transfer between $Ar^+(P\ 1/2)$ and $Xe^+(P\ 3/2)$.

To implement temperature control, a stainless steel gas cell was designed with heating and cooling capability. Its installation, which required modification of most of the other experimental hardware,has been completed and preliminary data is in hand.

BACKGROUND

In this section the electronic structure and transitions of rare gas atomic and molecular states are first reviewed. This is followed by a discussion of the properties of the heteronuclear rare gas ions and emission spectra of their electronically excited states. The discussion concludes with a simple kinetic model that illustrates how the initially anticipated molecular ion formation and decay rates might be extracted from time-resolved emission spectra. Though the preliminary data suggests a somewhat more complicated picture, the model presented should serve as an appropriate point of departure for unraveling the kinetics of these systems.

A. Atomic States

The heavy rare gases are Ne (10 electrons), Ar (18 electrons), Kr (36 electrons) and Xe (54 electrons). Each of these gases has the ground state configuration ns^2 np^6. When a p electron is removed and placed in a higher orbital an excited state is formed. One unit of angular momentum and one-half unit of spin is retained by the ionic core. Thus the ns^2 np^5 configuration of the core is split by its spin-orbit interaction into two energy levels, a 2P3/2 (lower) and a 2P1/2 (upper) state (see figure 1).

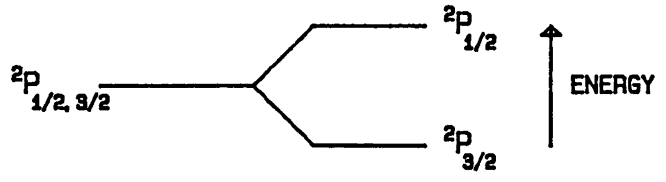

Figure 1. Splitting of states in core of rare gas atom.

The ordering of these two levels is given by the rule which states that multiplets formed from equivalent electrons are regular (sublevel with minimum J lies lowest) when less than half the shell is occupied, but inverted (sublevel with maximum J lies lowest) when more than half the shell is occupied; the latter case being applicable here. For a proof of this rule one is referred to Condon and Shortley [8].

Due to the strong spin-orbit coupling of the core, a rather unusual coupling scheme is applicable to excited states of rare gas atoms, particularly the heavier rare gas atoms. In this coupling scheme, after the core electrons form a total angular momentum j, the outer excited electron binds its angular momentum l to the total core momentum j, forming K. This K then couples with the spin, s, of the excited electron to form J, the total angular momentum of the atom. This unusual coupling scheme is called j-l coupling.

B. Homonuclear States

Inert or rare gases in their ground states do not generally attract one another. Since there is no valence force either of homopolar (atomic binding) or of heteropolar (ionic binding) kind acting between two normal inert gas atoms, the only possible attraction is the well known van der Waals force. This small attraction, due to polarization, only overcomes the strong repulsion of the zero-valent atoms at relatively large internuclear distances ($\geq$4A). London [9], calling these forces "dispersion forces", has shown them to be due to the perturbation of the repulsive ground state by the higher electronic states of the system consisting of the two atoms. This perturbation at large internuclear distances gives a potential energy decreasing as $-1/r^6$ toward smaller r values. The weak binding due to van der Waals forces only exists (appreciably) for the heavier, more polarizable rare gases such as Ne

and Ar but due to the resulting shallow potential well,these molecules (e.g., Ne2,Ar2) are not very stable.

In contrast to ground state rare gas atoms, an ionic ground state rare gas atom and a neutral ground state rare gas atom can form stable molecular states. For instance the binding energy is 1.1eV for $Ne2^+$ 1.4eV for $Ar2^+$ 1.2eV for $Kr2^+$ and 1.0eV for $Xe2^+$. Thus an addition of an outer electron in an orbital large compared to the internuclear separation,a so-called Rydberg orbital, about such bound molecular ions should form bound excited states. Such states were first described by Mulliken [10]. His estimates of the potential curves of $Xe2^+$ have proven to be invaluable to revealing the properties of rare gas molecules.

Although there has been other such qualitative work since Mulliken's,the first quantitative calculations were done by Cohen and Schneider [11] on neon. They obtained potential curves for Ne2 and $Ne2^+$ by first calculating wave functions ab initio,without the spin-orbit interaction and then including spin-orbit effects by a semi-emperical technique using atomic spectral data. Many calculations have been done since Cohen and Schneider's work,including calculations by Ermler et al.[12] for Xe2.

The success of calculations like that of Cohen and Schneider is based upon the ability to accurately merge calculations with and without spin-orbit coupling. Without such separate considerations, the calculations would be significantly more difficult. It is the unique nature of heavy rare gas atoms which makes this treatment successful. The effects of spin-orbit coupling are rather small in comparison to Coulombic interactions in light atoms, particularly the alkalis. This is due to the rather complete shielding that electrons in such atoms create. However,as the size of the atom increases or Z increases, the orbiting electrons are more densely packed,resulting in less

and less electronic shielding. This enables spin-orbit coupling to equal and eventually (with increasing Z) overcome the residual Coulomb interaction. Thus, for the heavier rare gas atoms, spin-orbit effects are important in the core. However, the fact that there is a particularly large energy difference between every s subshell and the preceding p subshell is very important when considering excited states of rare gases. In rare gases the p subshell is just completed. Because of the considerable difference between the energy of an electron in the p subshell and the energy it would have if it were in the s subshell, the first excited state of these atoms is unusually far above the ground state. As a result, the excited electron sees a very shielded core and thus, experiences relatively weak spin-orbit effects. This explains the rather strange j-l coupling scheme applicable to heavy rare gas atoms. Since the excited or valence electrons are responsible for chemical bonding of the rare gas atoms, but are subject to negligible spin-orbit effects, whereas spin-orbit effects are only significant in the core of these atoms, it seems reasonable to consider valence forces and spin-orbit effects separately. Such an argument was briefly presented by Cohen and Schneider [11].

The best description for the heavy rare gas molecules is given by Hund's case c [13]. It is analogous to the j-l coupling applicable to rare gas atoms. In case c, the interaction between L and S may be stronger than the interaction with the internuclear axis and thus Λ and Σ are not defined; rather, L and S first form a resultant Ja, which is then coupled to the internuclear axis with an axial component, Ω. The electronic angular momentum, Ω and the angular momentum N, of nuclear rotation, then form the resultant angular momentum J. Figure 2 is a vector diagram for Hund's case c. The precessions of L and S about Ja and of Ja about the line joining the nuclei are not indicated.

As mentioned earlier, the method for qualitatively determining molecular

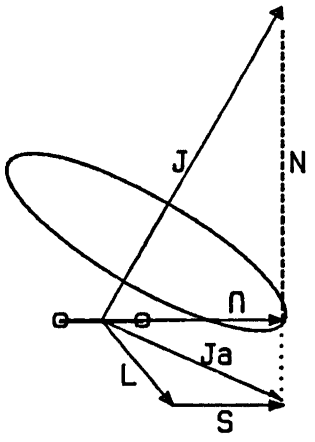

Figure 2. Vector diagram for Hund's case c.

states and potential curves of homonuclear diatomic rare gases was originated by Mulliken [10]. This method calls for first combining a rare gas ion. denoted Rg and the neutral rare gas atom Rg. The addition of an electron in a Rydberg orbital then completes the molecule or dimer as it is called.

$$Rg^{+} + 2Rg \rightarrow Rg2^{+} + Rg$$

$$Rg2^{+} + e^{-} + Rg \rightarrow Rg2 + Rg$$

This process incorporates the separated-atom method for building up molecules; that is the molecular states are determined from given states of the separated atoms. Since the neutral rare gas atom has outer configuration np^6,it is in a 1S0 state, having zero angular momentum and one-half unit of spin. The ion, having configuration np^5, has one unit of angular momentum and one-half unit of spin. The total angular momentum of the ion can thus be either J=3/2 or J=1/2 which yield states 2P3/2 or 2P1/2. Consequently,there are two separated atom limits; 2P3/2 + 1S0 and 2P1/2 + 1S0. Using the rules of Hund's case c, we can determine the corresponding states. For separated atom limit 2P3/2 + 1S0 , J(neutral)=0 and J(ion)=3/2. So Mj(neutral)=0 and Mj(ion)=3/2,1/2,-1/2 and -3/2. Since $\Omega = |Mj1 + Mj2|$ we get Ω=1/2,3/2. Now since we are combining like atoms ,that is, the nuclei have the same charge,symmetry indicates that

each state occurs twice, once as an odd and once as an even state. Thus the corresponding states for the separated atom limit 2P1/2 + 1S0 are a 1/2 u and a 1/2 g. If one computes possible molecular states, ignoring spin-orbit coupling, the resulting states can be correlated to the Hund's case c states. For the neutral atom Rg, the 1S0 state has M=0, whereas the ion, Rg^{+}, has M=1, 0, -1. Therefore Λ =1, 0 and since Σ = 1/2, the resulting molecular orbital (MO) substates are 2Σ 1/2, 2Π 3/2, 2Π 1/2, not including symmetry. As taken from Mulliken [10], the MO substates $A2\Sigma$ 1/2u, $B2\Pi$ 3/2g, $B2\Pi$ 1/2g, and $C2\Pi$ 3/2u derive from 2P3/2 + 1S0 and $C2\Pi$ 1/2u and $D2\Sigma$ 1/2g derive from 2P1/2 + 1S0, as shown in figure 3.

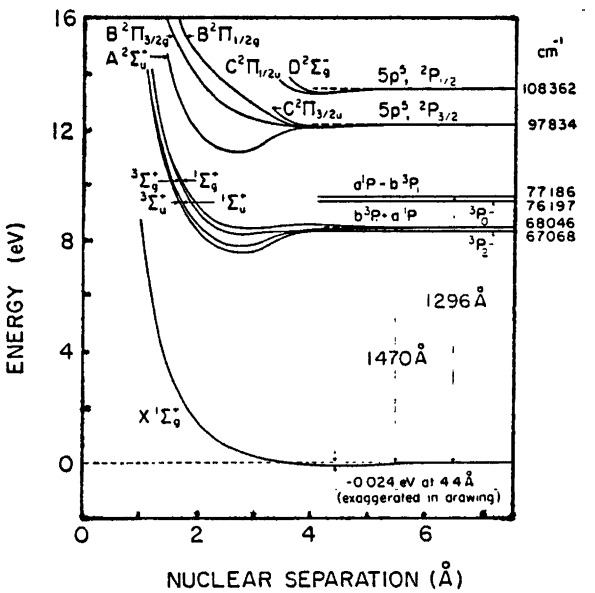

Figure 3. Mulliken's estimated potential curves for Xe2.

At large R values the 1/2u wave functions from 2P3/2 + 1S0 and 2P1/2 + 1S0, respectively, are mixtures of $A2\Sigma$ 1/2u and $C2\Pi$ 1/2u, while, as R decreases, the lower and upper 1/2u states must increasingly approach pure $A2\Sigma$ 1/2u and pure $C2\Pi$ 1/2u states, respectively. However, even at Re (equilibrium separation)

of the groundstate of Rg2 (in this case Xe2), the purification is definitely not complete. Similar considerations apply to the two 1/2g states. However, the 3/2g and 3/2u states are pure B2TT 3/2g and pure C2TT 3/2u at all R values. Thus, we see that the inclusion of spin-orbit coupling mixes Σ and TT states though not the TT 3/2 states.

In contrast to the qualitative work of Mulliken, the quantitative calculations of Cohen and Schneider [11] on Ne2 and $Ne2^+$ included extensive ("the number of configurations included was typically about 30") ab initio configuration-interaction calculations. The potential curves resulting from similar calculations, more recently produced by Ermler [12] et al. for Xe2 and $Xe2^+$ are illustrated in figure 4.

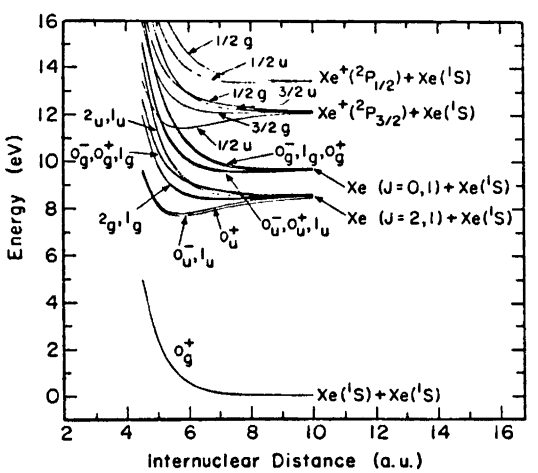

Figure 4. Calculated potential curves for Xe2 and $Xe2^+$ as produced by Ermler et al. [12].

C. Rare Gas Spectra

The lowest bound molecular states of the rare gases are a 0_u^+ and a 1_u state, as can be seen from the previous figures. Radiation from these states to the repulsive ground state gives rise to the broad unresolved VUV (vacuum ultraviolet) continua of the rare gases. The molecular spectra of the heavier rare gases in the vacuum ultraviolet seem to all follow a similar pattern. Most outstanding is a continuous emission region extending from very near the first resonance line toward longer wavelengths. (The resonance line is known as the longest wavelength capable of exciting fluorescence for the atom). This continuum shows two major peaks commonly referred to as the "first continuum"- closer to the resonance line- and the "second continuum"- at longer wavelengths. At pressures of about one Torr, the spectrum shows the atomic resonance lines with line widths which are significantly pressure broadened. As the pressure is increased, the emission due to the lower resonance state becomes asymmetrically broadened toward longer wavelengths, with the peak also shifting somewhat toward the red. This emission feature is the first continuum since it appears at fairly low pressures and has no resolved structure.

At pressures greater than about 100 Torr, the well resolved second continuum emission appears at slightly longer wavelengths than the first continuum. Increasing the pressure causes the second continuum to become more intense while the first continuum diminishes. The atomic emission spectra also becomes weak at these pressures. Eventually, for pressures greater than about 1000 Torr the only emission feature in the VUV is the second continuum. The second continuum has been identified by Tanaka [13] et al. as emission from 0_u^+ and 1_u molecules in their lower vibrational levels to the repulsive ground state. The continuum width is entirely due

to the slope of the ground state potential curve. At high pressures,where the first continuum does not interfere, its line shape is more or less Gaussian and symmetrical.[14]

The first continuum is attributed to radiation from high vibrational states of the rare gas molecule. High vibrational states can radiate from either side of the potential well. The outer edge would therefore correspond to radiation at slightly longer wavelengths than the atomic line,since the ground state potential curve is just beginning to rise at that internuclear distance. Radiation from the inner edge would give rise to light of much longer wavelength. This has been suggested as the reason for the broad weak continua found in the visible or near ultraviolet for the pure rare gases.[15] Figure 5 shows the first and second continuum emissions for Ar2.

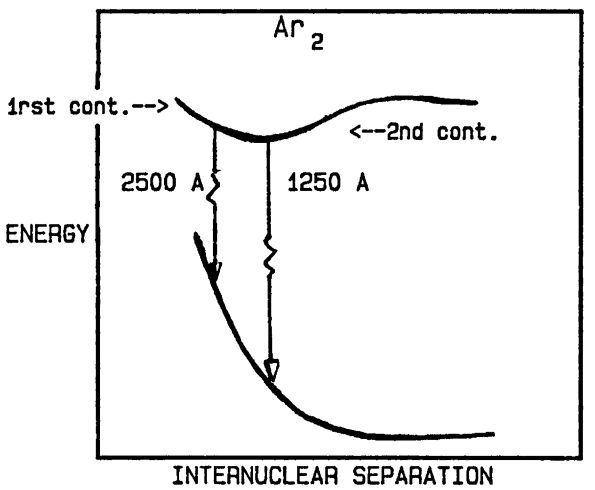

Figure 5. First and second continuum emissions for Ar2.

D. Heteronuclear Molecular States

The binding between the rare gas atoms in a homonuclear molecule is essentially due to the "exchange degeneracy"- that is the fact that for very large internuclear distance, by exchange of the two electrons of the two atoms, a configuration results that is indistinguishable from the original

configuration. As a result, when the two atoms approach each other, an interaction between them arises which can be mathematically described in terms of "electron exchange" and which leads to a splitting into two states of different energy. For this reason the homopolar forces between two neutral atoms are sometimes also called "exchange forces." The exchange forces are attractive for antiparallel spin orientation and repulsive for parallel spin orientation of the electrons. However, it must be emphasized that the strong attraction (or repulsion) is not due to the mutual interaction of the spins, which is very weak. The spin comes in only through its effect on the Pauli principle. It acts as a sort of indicator for the sign of the interaction of the atoms. This is similar to the relation of the spin to the energy difference of singlet and triplet states of the same electron configuration. Ionic homonuclear dimers experience a similar binding effect at large internuclear separation, known as resonance degeneracy, because the state "electron with the one nucleus" has the same energy as the state "electron with the other nucleus". [16]

Since there is no resonant exchange interaction for heteronuclear molecules, the binding energy of the excited or ionized heteronuclear molecules will be considerably smaller than their homonuclear counterparts. Though there has recently been much experimental interest in heteronuclear diatomic molecules, as particularly evidenced by the seminal work of Tanaka [3] et al., the only theoretical calculations to date have been those of Bender and Winter [17] for the heteronuclear molecular ion states of $(ArKr)^+$. Their potential curves are reproduced in figure 8. The notation is still that of Hund's case c, but the u/g symmetry is no longer applicable. Since there are no Ω=0 states, the +/- symmetry is not distinguishable either. In addition, all of the states have Ω values within + or - 1 of

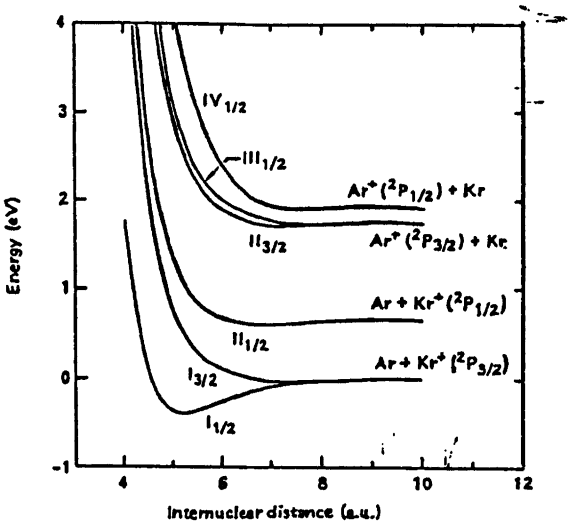

Figure 6. The potential curves of Bender and Winter [17] for $(ArKr)^+$.

each other. Thus there are no symmetry or angular momentum selection rules to govern the optical transitions among these levels. This agrees with the spectroscopic results of Tanaka et al. who saw optical transitions among these states in several binary rare gas mixtures. In fact, Tanaka et al. observed that nine of the ten binary mixtures of He, Ne, Ar, Kr and Xe, when excited in an electrical discharge, emitted one or several broad bands which were unique to the mixture. The emissions do not exist under like conditions for any of the pure rare gases. It was discovered that each of these bands peaked near a wavelength which corresponded to the energy difference between one of the atomic ion levels of the lighter rare gas atom and one of the atomic ion levels of the heavier rare gas atom. It was also recognized that similar bands had been seen earlier in Ar/Kr, Ar/Xe and Kr/Xe mixtures by Friedl [4] and Kugler [5] using high energy electron beam excitation.

Though these earlier experimentalists had attributed the bands to neutral heteronuclear molecule emissions, the bands they discovered were consistent with the suggestion of Tanaka et al., that they involved ion levels. Tanaka et al. argued that since the bands were broad and in general

contained well defined vibrational progressions, the emissions involved transitions of the heteronuclear molecular ions

$$Rg1Rg2^{+} \rightarrow Rg2Rg1^{+} + h\nu ,$$

where Rg2 has the higher ionization potential. Though not all of the transitions possible within this model were seen, all of the unique emissions of the mixtures fit the model well. Since there are no angular momentum or symmetry rules to select optical transitions, nearly any transition is possible. One might expect them to occur not only for excitation techniques, such as electrical discharges, but also for high energy electron impact, since both produce an abundance of ions. In fact, similar bands have been detected in several rare gas mixtures excited by high energy electrons at Rice University (e.g., Ar/Xe and Kr/Xe mixtures) [18]. Figure 7 illustrates the potential curves and transitions between them with and without spin-orbit coupling. In this case, the mixture of lighter Ar to heavier Xe is shown. Open shell-closed shell and closed shell-closed shell molecular orbital diagrams indicate why $p\sigma$ - $p\sigma$ coupling is stronger than $p\sigma$ - $p\pi$ coupling. This implies that states with predominantly Σ character should make strong transitions. In fact, Bender and Winter [17] calculated the transition A, IV 1/2 --> I 1/2 to be the strongest. This along with most of the transitions has both $\Sigma - \Sigma$ and $\Sigma - \Pi$ components.

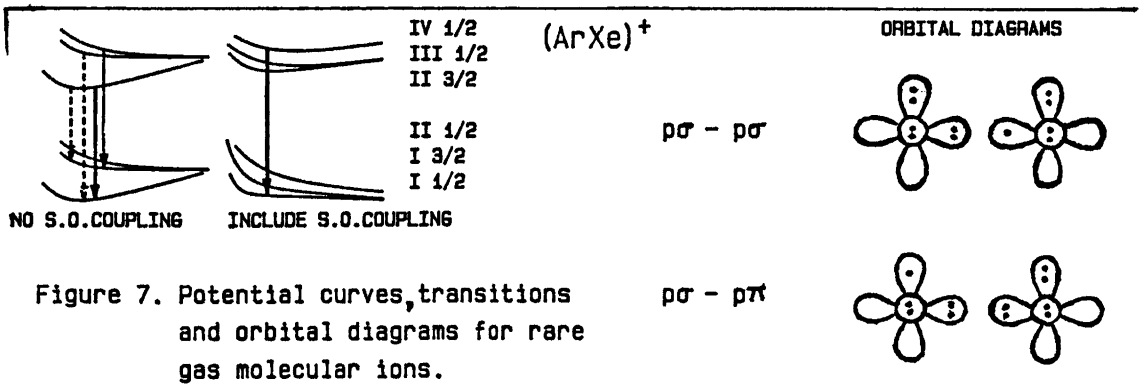

Figure 7. Potential curves, transitions and orbital diagrams for rare gas molecular ions.

Prior to running the present experiment, a spectral analysis was performed for different mixtures of Ar/Xe. At a total pressure of about 600 Torr, with a mix ratio of 10/1, an intense fluorescence line at 3280 A was seen after high energy electron excitation of Ar/Xe. This corresponds to the A transition shown by Tanaka et al.[3] to be at 3255.6 A. Figure 8 illustrates this peak. The small broad structure to the left of the $(ArXe)^+$ line is attributed to the second continuum of xenon, observed in second order.

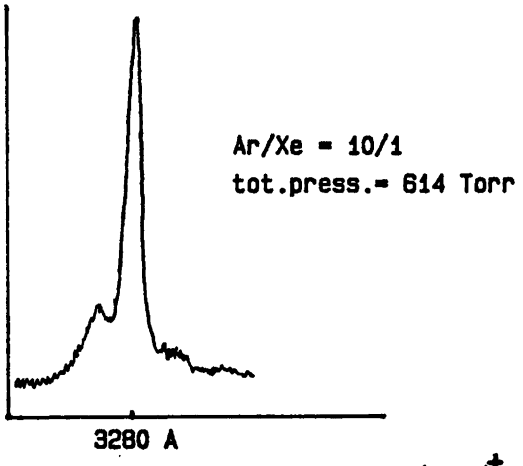

Figure 8. Intense fluorescence line of $(ArXe)^+$ at 3280 Å

E. Prototype Kinetic Model

In order to interpret time-dependent spectral data from systems such as those described above, one must have a model that incorporates all the pertinent kinetic processes. One starts by listing potential reactions of the involved species. Retaining the most important of these reactions, standard reaction rate principles can be applied to yield a system of differential equations. Solution of these equations should give an analytical description of the data.

The basic processes in this experiment are the following:

1) $e^- + Ar \rightarrow Ar^+ + 2e^-$

2) $Ar^+ + Xe + Xe \xrightarrow{k1f} (Ar^+Xe) + Xe$

3) $Ar^+ + Xe + Xe \xleftarrow{k1d} (Ar^+Xe) + Xe$

4) $Ar^+ + Xe + Ar \xrightarrow{k2f} (Ar^+Xe) + Ar$

5) $Ar^+ + Xe + Ar \xleftarrow{k2d} (Ar^+Xe) + Ar$

6) $Ar^+ + Xe \xrightarrow{R} Ar + Xe^+ + h\nu\,(325nm)$

7) $(Ar^+Xe) \xrightarrow{A} (ArXe^+) + h\nu\,(328nm)$

8) $Ar^+ + Xe + e^- \xrightarrow{r1} Ar^{**} + Xe$

9) $Ar^+ + Ar + e^- \xrightarrow{r2} Ar^{**} + Ar$

Process number one describes the formation of argon ions by electron beam impact. The next four processes represent three-body formation and two-body destruction of the excited $(ArXe)^+$ ions. Process number six is radiative charge transfer by atomic collisions and number seven is radiative decay of the molecular ion. Both eight and nine are recombination processes.

Numbers 1, 8 and 9 need not be included. Process 1 occurs almost instantaneously, implying that the argon ions are present at time t=0. The last two processes of recombination can be made negligible by keeping the concentration of electrons low.

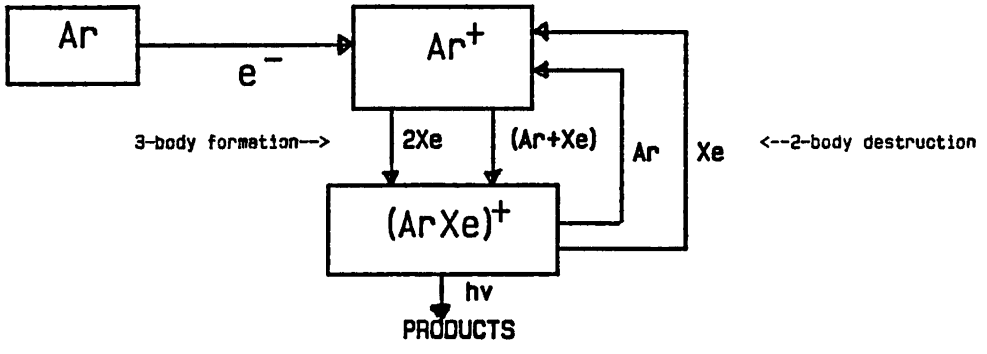

Figure 9. Block diagram of kinetic processes, excluding charge-transfer.

The remaining processes yield the following differential equations:

(a) $d[(Ar^+Xe)]/dt=k1f[Ar^+][Xe]^2-k1d[(Ar^+Xe)][Xe]+k2f[Xe][Ar][Ar^+]-k2d[(Ar^+Xe)][Ar]-A[(Ar^+Xe)]$

(b) $d[Ar^+]/dt=-k1f[Ar^+][Xe]^2+k1d[(Ar^+Xe)][Xe]-k2f[Xe][Ar][Ar^+]+k2d[(Ar^+Xe)][Ar]-R[Ar^+][Xe]$

Now group terms:

(a) $d[(Ar^+Xe)]/dt=a[Ar^+]-(b+A)[(Ar^+Xe)]$

(b) $d[Ar^+]/dt=b[(Ar^+Xe)]-(a+R[Xe])[Ar^+]$

Where

$a=(k1f[Xe]^2+k2f[Xe][Ar])$

and

$b=(k1d[Xe]+k2d[Ar]+A)$

This system is readily solved by Laplace Transform:

(a) $sL([(Ar^+Xe)])-[(Ar^+Xe)]_0=aL([Ar^+])-(b+A)L([(Ar^+Xe)])$

At $t=0$ $[(Ar^+Xe)]=0$ or $[(Ar^+Xe)]_0=0$

==>

(a) $L([Ar^+])=(s+b+A)/a\ L([(Ar^+Xe)])$

Likewise

(b) $sL([Ar^+])-[Ar^+]_0=bL([(Ar^+Xe)])-(a+R[Xe])L([Ar^+])$

==>

(b) $L([Ar^+])=([Ar^+]_0+bL([(Ar^+Xe)]))/(s+a+R[Xe])$

If we equate (a) and (b) the result is:

(c) $L([(Ar^+Xe)])=([Ar^+]_0a)/((s+d)^2+c))$

Where

$d=(a+R[Xe]+b+A)/2$

and

$c=(b+A)(a+R[Xe])-ba-(a+R[Xe]+b+A)/4$

Taking the inverse transform of equation (c) yields the following result for the concentration of (ArXe) molecular ions as a function of time:

(d) $[(Ar^{+}Xe)] = a[Ar^{+}]_{0}/(\lambda_{+}-\lambda_{-})(\exp(-\lambda_{-}t)-\exp(-\lambda_{+}t))$

Where

$\lambda = (a+R[Xe]+b+A) +/- ((a+R[Xe]+b+A)^{2}-4(Rb[Xe]+Aa+RA[Xe]))^{1/2}/2$.

and as defined earlier,

$a = (k1f[Xe]^{2}+k2f[Xe][Ar])$

and

$b = (k1d[Xe]+k2d[Ar]+A)$.

Assuming k1f=k2f and k1d=k2d, shorter notation for a and b would be:

$a = kf[Xe][Xe+Ar]$

and

$b = kd[Xe+Ar]$.

Assuming that the given kinetic processes are correct, equation (d) is the exact solution. This solution yields a peaked curve for the time dependence of the 328nm fluorescence radiation, having a single exponential rise and a single exponential fall. The time constant of the rise is the larger of λ_{+} and λ_{-}, whereas the time constant of the fall is the smaller of λ_{+} and λ_{-}. This can be seen by considering the following:

The time rate of change of $[(Ar^{+}Xe)]$ is

$d[(Ar^{+}Xe)]/dt = a[Ar^{+}]_{0}/(\lambda_{+}-\lambda_{-})(-\lambda_{-}\exp(-\lambda_{-}t)+\lambda_{+}\exp(-\lambda_{+}t))$

or

$d[(Ar^{+}Xe)]/dt = A1\ \exp(-\lambda_{-}t) + A2\exp(-\lambda_{+}t)$

Where

A1 varies as $\lambda_{-}/(\lambda_{-}-\lambda_{+})$

and

A2 varies as $\lambda_{+}/(\lambda_{+}-\lambda_{-})$

The amplitudes A1 and A2 determine which of the two exponential components λ_+ and λ_- governs the rise and which the decay of the fluorescence. If λ_- is greater than λ_+, then A1 is positive and A2 is negative. Thus λ_- is the time constant of the rise and λ_+ is the time constant of the fall. Likewise, if λ_+ is greater than λ_-, the opposite is true.

Physically meaningful approximations for λ can be obtained by considering limiting cases. Before considering such cases, a preliminary simplification can be made by noting that radiative charge transfer rates are generally much smaller than the other rates being considered. On this basis, we ignore terms proportional to R, yielding:

$$\lambda = (a+b+A) \pm ((a+b+A)^2 - 4Aa)^{1/2}/2$$

CASE 1:

In case (1) we assume that there is negligible collisional destruction of the $(ArXe)^+$ ion (i.e. $kf[Xe] \gg kd$). This implies that $b \ll a$. Thus ==>

$$\lambda = (a+A) \pm ((a+A)^2 - 4Aa)^{1/2}/2$$

or

$$\lambda = (a+A) \pm (a-A)/2$$

Thus

$$\lambda_+ = kf[Xe][Xe+Ar]$$

and

$$\lambda_- = A.$$

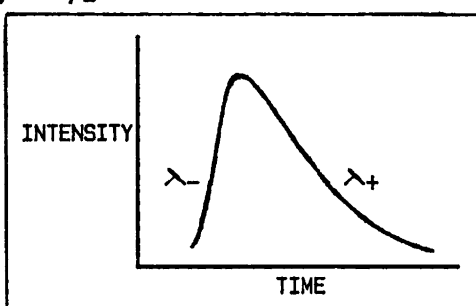

Figure 10. Time dependent curve for case (1).

It so happens that the work of Millet et al. [7] appears to agree with this limiting case (1), assuming λ is the rise. They reported seeing three-body decay (λ_+) and a rise too short to measure.

CASE 2:

In case (2), let us maintain collisional destruction and assume it to be much faster than the other processes. This is equivalent to saying that

b>>A a. We proceed by factoring (a+b+A) out of the square root term in λ and making an expansion which neglects small terms:

$$\lambda = (a+b+A) \quad +/- \quad ((a+b+A)^{2} - 4Aa)^{1/2} /2$$

$$\lambda = (a+b+A) \quad +/- \quad ((a+b+A)^{2} (1-4Aa/(a+b+A)^{2}))^{1/2} /2$$

$$\lambda = (a+b+A) \quad +/- \quad (a+b+A) (1-4Aa/(a+b+A)^{2})^{1/2} /2$$

Now expand the square root.

$$\lambda \cong (a+b+A) \quad +/- \quad (a+b+A) \quad (1-2Aa/(a+b+A)^{2}) \; /2$$

$$\lambda \cong (a+b+A) \quad +/- \quad (a+b+A) \quad - \; 2Aa/(a+b+A) \; /2$$

Since b>>A ,a, we can neglect a and A in the denominator of 2Aa/(a+b+A) .==>

$$\lambda \cong (a+b+A) \quad +/- \quad (a+b+A) \; - \; 2Aa/b \; /2$$

Thus

$$\lambda_{+} \cong kd[Xe+Ar]$$

and

$$\lambda_{-} \cong A \; (kf/kd) \; [Xe]$$

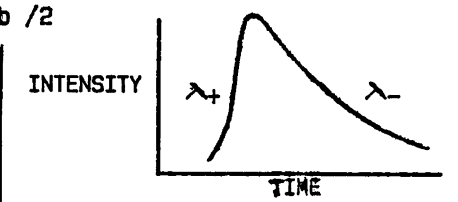

Figure 11. Time dependent curve for case (2).

Having assumed b or kd[Xe+Ar] to be the dominant term, λ_{+} must be the rise time constant, representing two-body destruction, and λ_{-} the fall time constant, representing radiative decay of the fraction of bound molecular ions.

As will be shown later, neither of these cases agree with the preliminary data of this work. However, as noted above, case (1) is, in fact, the model proposed by Millet et al. after performing a similar experiment with $(ArXe)^{+}$. Likewise, case (2) has been shown by Bonifield [19] to describe the time dependence of preliminary data on the 490nm $(KrXe)^{+}$ emission.

EXPERIMENTAL APPARATUS AND TECHNIQUES

A. Basic Method

The experimental apparatus consists basically of a 160KeV electron linear accelerator which sends electrons down an evacuated beam tube through a metal foil into a gas chamber. Experimentally, there are two modes of operation. The first involves spectral analysis; the second, time resolution.

When obtaining spectral data, a steady beam of electrons is accelerated into the gas chamber or cell. The intensity of resulting gas fluorescence is measured by a photomultiplier tube on the end of a monochromator which scans the spectrum of the fluorescence. This way, emission bands of the excited gas species can be recorded.

This particular experiment utilizes the second mode, time resolved spectroscopy. In this mode, the apparatus is used to study the time dependence of a particular excited state or emission band. While traversing the beam tube, the accelerated electrons pass through parallel metal plates across which a square wave voltage forces them to be swept past the foil aperture in a sub-nanosecond time interval. Fluorescence from the excited gas species is passed by an optical filter of selected wavelength into a photomultiplier tube. By measuring the time interval between gas excitation (as electrons are swept by the foil) and the arrival of light to the photomultiplier tube (P.M.T.) over many cycles, a statistical distribution of the excited state intensity can be recorded as a function of time with nanosecond resolution.

B. Detection Technique

Because this experiment uses a low intensity electron beam as an excitation

source, the ability to detect small signals is needed in order to extract useful information from the system. Therefore, the single photon counting technique has been adopted, as it is best suited for the measurement of low level optical signals.

Basically, the technique involves repeated excitation of the gas sample such that at most, one photon is detected per experimental cycle. The probability of detecting a photon at any given time is proportional to the number of radiating states present in the sample. Therefore, the time of arrival distribution of photons is proportional to the time dependence of the number of radiating states. The nature of the electronic detection system restricts the photon counting by measuring the time interval between the excitation of the sample and the arrival of the first photon, ignoring subsequent photons. Detection of more than one photon per cycle distorts the time of arrival distribution,since timing information is only obtained for the first photon.

A block diagram of the entire experiment is provided in figure 12.

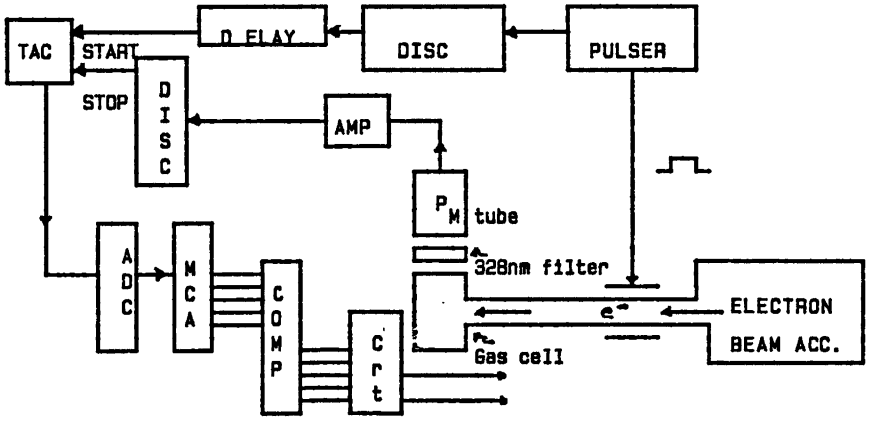

Figure 12. Experimental setup.

C. Apparatus

The electron beam is generated by a Cockcroft-Walton accelerator with a voltage potential of 160KV and a maximum measured current of 250 μa. Electrons flowing through a tungsten filament are extracted by a circular focusing anode and accelerated by several similar accelerating anodes to an energy of 160 KeV, where they emerge into a meter long beam tube. As the electrons travel down the beam tube, they go through, in order, vertical steering plates, horizontal steering plates, vertical pulsing plates, and another pair of horizontal steering plates. After another 30 cm, the electron beam enters the gas cell through a disc of Havar foil covering a 1/4 cm diameter hole. The purpose of the foil is to separate the beam tube vacuum (10^-7 Torr) from the pressurized gas cell without deterring the path of the electron beam. Once inside the gas cell the electrons deposit their energy into the gas mixture, creating ions and excited states.

The vertical pulsing plates are used to sweep the electron beam past the aperture. The pulse applied to the plates is generated by discharging a length of 50 ohm coaxial cable through a spark gap. The dimensions of the deflection plates are such that they constitute a 50 ohm stripline and they are terminated with a 50 ohm resistor to prevent reflection. The pulse appearing on the plates is shown in figure 13. The beam is swept past the aperture twice, once as the voltage pulse rises, and once as it falls. The beam was steered into a position such that deflection past the gas cell aperture was effected by the steepest parts of the leading and trailing edges; thus the ringing of the pulse near the peak and slow decay near the baseline did not affect excitation of the gas sample. As shown in the figure, the slew rate of this part of the pulse is greater than 300V/nsec. Since only 100 volts are required to sweep the beam past the aperture the

Figure 13. Pulse applied to deflection plates. The lower portion of the figure is an expansion of the trailing edge of the square pulse shown above.

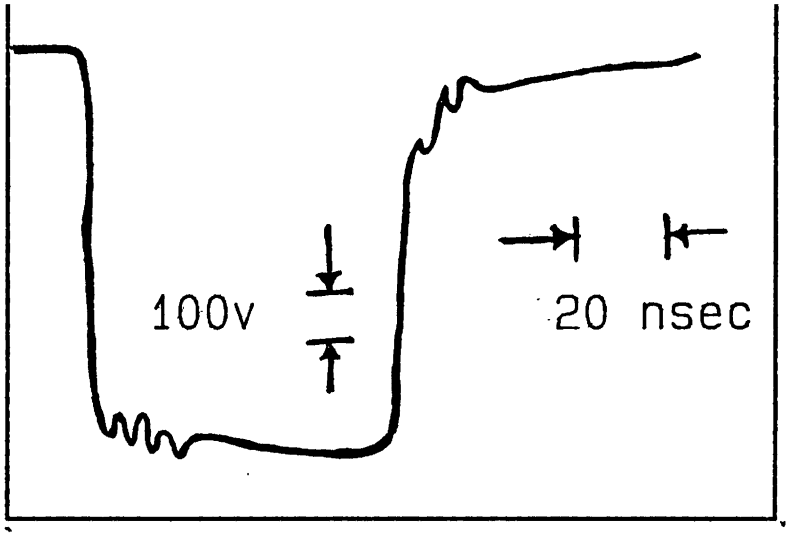
100v
20 nsec

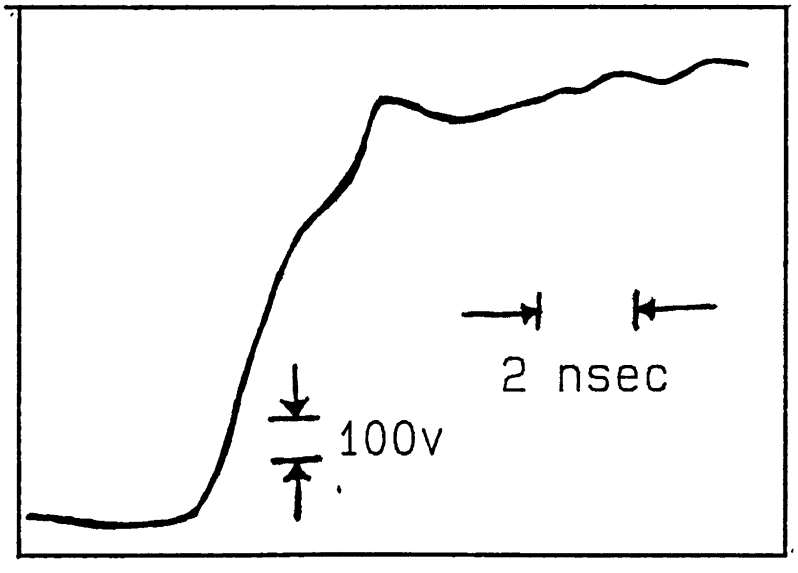
2 nsec
100v

duration of the current pulses entering the gas cell is less than one nsec.

It was shown by Gleason [20] that double excitation due to the rise and fall has no effect on the time constants and has little effect on the amplitudes of terms having time constants much less than 100 nsec.

As shown in figure 12, an inductive pickoff is used to generate a timing signal from the pulser, which starts the time-to-amplitude converter (TAC). The optical interference filter is used to select photons of the proper wavelength prior to detection by the photomultiplier (RCA 8850). The anode signal from the photomultiplier is used to stop the TAC. The discriminator used is of the constant fraction type which eliminates error due to variations in the height of the anode pulse and enables timing resolution which is considerably better than the 1.5 nsec risetime of the anode pulse. The output from the last dynode of the photomultiplier is proportional to the number of photons striking the photocathode. By integrating this signal, one can obtain the number of events detected by the photomultiplier over the desired time interval. This is accomplished by the amplifier shown in the figure. The analog-to-digital converter can then be gated if the integrated dynode pulse indicates that one photon has been detected during the chosen time interval. During this experiment, however, gating of the analog-to-digital converter was considered unnecessary, since the signal count rates were low enough (100 cts/sec) to make multiple photon events improbable. Noise pulses in the photomultiplier can also be discriminated against, since they will result in dynode pulses of lower voltage than those corresponding to single photons. The analog-to-digital converter is interfaced to a multichannel analyzer (MCA), which, in turn, is interfaced to a computer. This arrangement allows for storage and analysis of the data.

The gas manifold is shown in figure 14. This system consists basically of a gas cell which contains the sample gas mixture two gas bottles and a mixing bottle. The manifold is rough pumped by a cryopump (sorption pump) and then pumped to 10^-9 Torr by an ion pump. The mass spectrometer is used to monitor the species of impurities present while the cell is being pumped. Water vapor, which is the most prominent impurity, is removed by baking the system. The entire manifold including the gas cell was constructed with stainless steel.

The gas cell which was designed especially for this experiment is pictured in the assembly drawing in figure 15. There are four ports numbered in the drawing. Port 1 is where the electron beam enters the cell. The arrow at (a) shows the face on which the Havar foil is silver soldered. Port 2 has attached a thermocouple feedthru, containing two pairs of thermocouple wire (copper and constantan) used to measure the gas temperature. As shown in the figure, ports 3 and 4 are faced with mini conflat flanges containing magnesium fluoride windows. These windows are surrounded by tubing which allows for placement of optical filters. The The P.M.T. can then be mounted on external flanges to view fluorescent light, either perpendicular to the beam's path as at 3,or parallel to the beam's path as at 4. The arrow at (b) shows the entrance to the cell to which the gas manifold is attached.

Cooling of the gas is achieved by flowing cold nitrogen gas through copper tubing wrapped around and soldered to the cell. The nitrogen gas is cooled as it flows through coiled copper tubing submersed in a dewar of liquid nitrogen. By varying the flow rate of the nitrogen gas, the gas temperature can be regulated at low temperatures.

Heating of the gas is done by electric heating tape wrapped about the

Figure 14. Gas manifold.

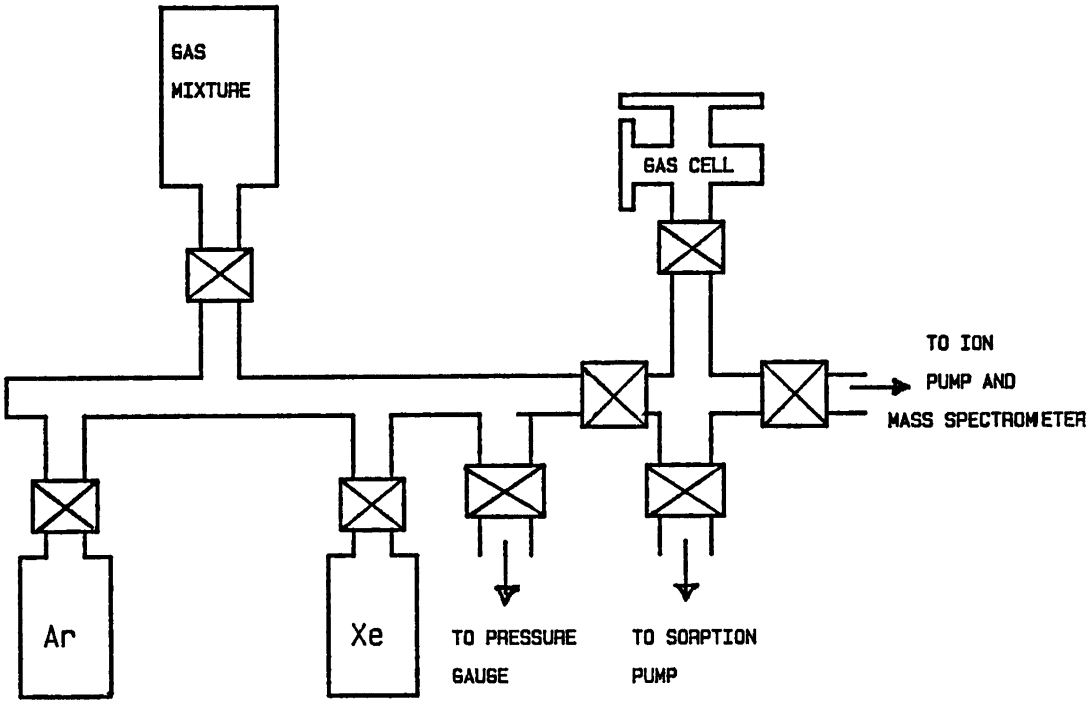
GAS
MIXTURE
GAS CELL
TO ION
PUMP AND
MASS SPECTROMETER
Ar
Xe
TO PRESSURE
GAUGE
TO SORPTION
PUMP

cell. Regulation of the heat is attained by powering the heating tape with a variac, which varies the voltage across the tape. The entire gas chamber is covered with insulation to better assure uniformity of the cell temperature.

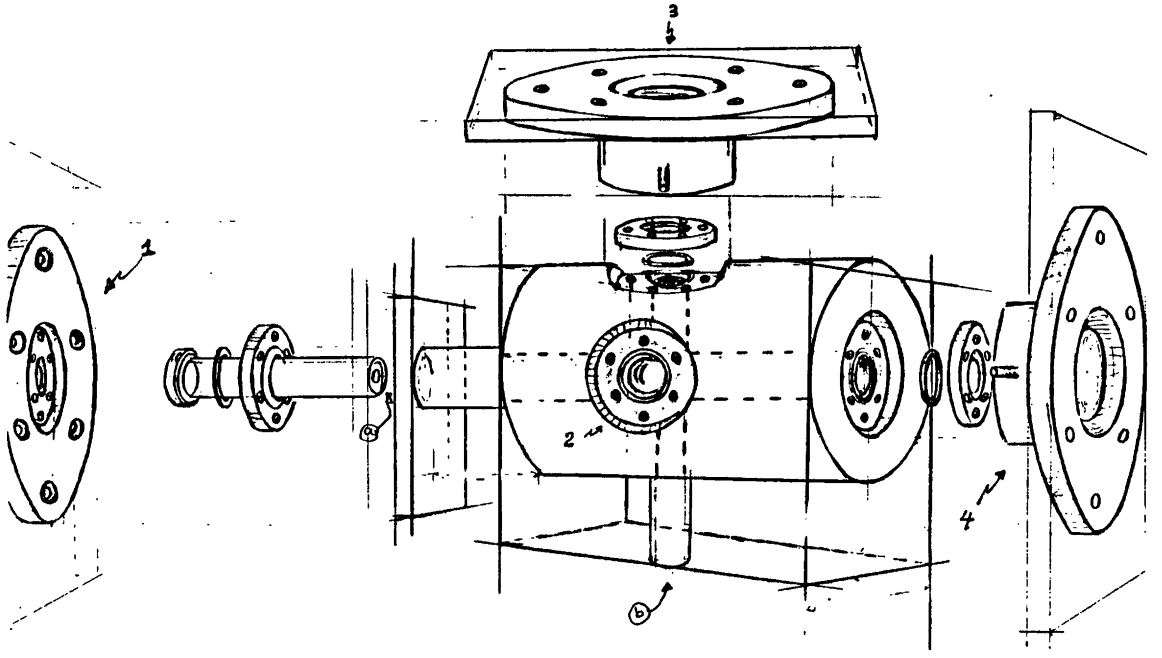

Figure 15. Assembly drawing of gas cell.

EXPERIMENTAL RESULTS

Preliminary time resolved data taken at various gas temperatures visibly demonstrate the strong temperature dependence of the spectra. Figure 16 shows spectra for four different temperatures taken on an 800 ns time scale. Not shown is a spectrum at T=248K which was taken on a shorter time scale (100 ns), due to the small time constant of the decay. The gas mixture consisted of 20 Torr argon and 480 Torr xenon for a total pressure of 500 Torr at room temperature. Although spectral studies indicate higher 328nm emission intensities for larger percentages of argon in the gas mixture, the decay constants become too long to measure in this regime. Thus, a convenient gas mixture with higher xenon pressure was chosen so as to facilitate data taking. Measurements with other gas mixtures are thus far incomplete,but consistent with the data on this mixture.

There are several interesting features about the spectra. First of all, there appears to be a fast but measurable rise component with a time constant on the order of a few nanoseconds. Secondly, another fast component with similar time constant seems present at the onset of the decay. This component is relatively weak, but prominent, particularly at higher temperatures. The strongest feature is a relatively long decay component on the order of a 100 ns. It is this long component which demonstrates the strong temperature dependence. Its time constant, which is approximately 150 ns at room temperature (298K) changes by almost 100 per cent over a hundred degree temperature range. This is illustrated in figure 17, which shows the long decay time constant as a function of temperature.

The room temperature data seems to agree with that of Millet et al. [7].

Figure 16. Time resolved spectra for different temperatures. The plots were originally on the same intensity scale but are shifted here to facilitate comparison of the decay components.

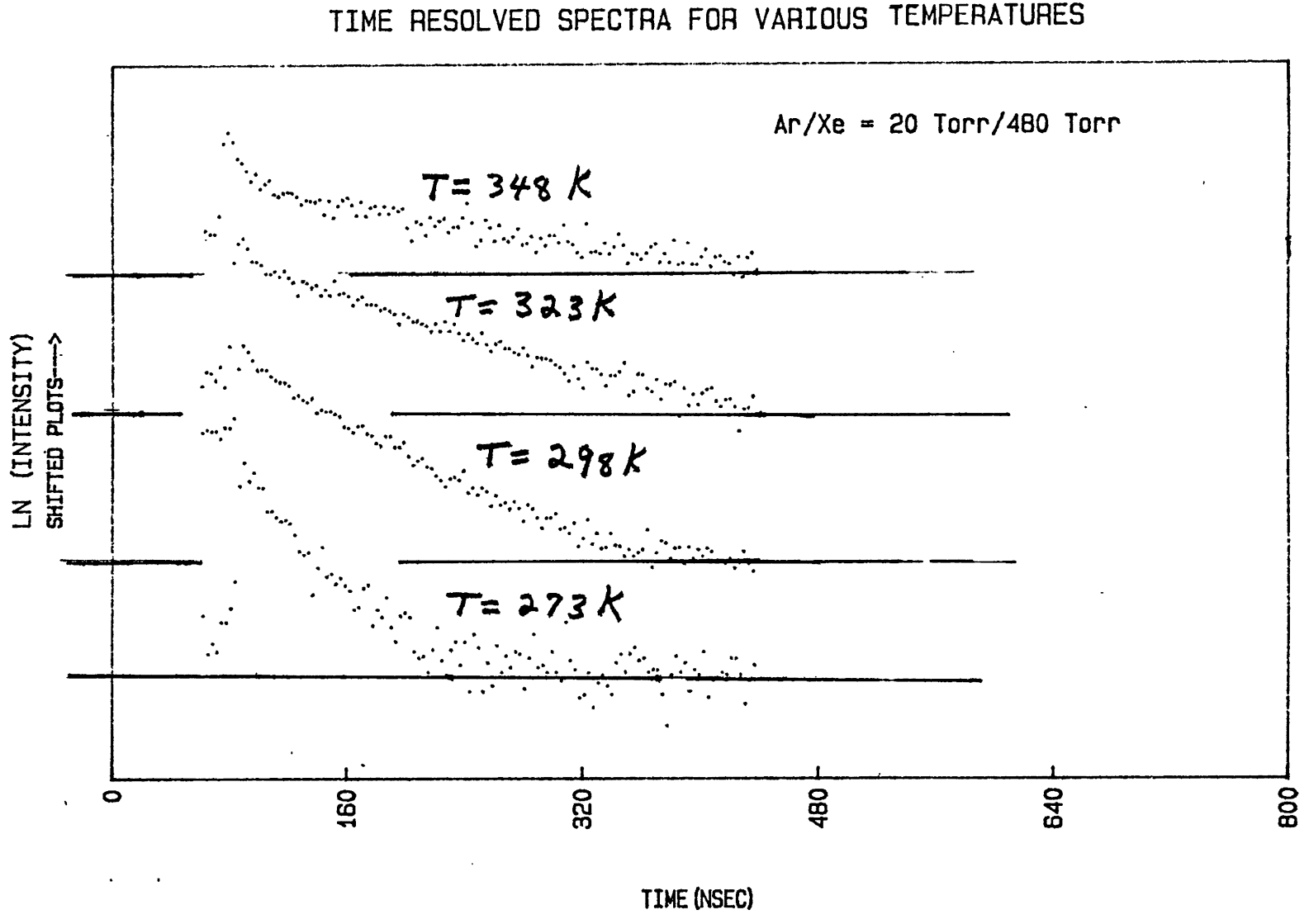
TIME RESOLVED SPECTRA FOR VARIOUS TEMPERATURES
Ar/Xe = 20 Torr/480 Torr
T= 348 K
T= 323 K
T= 298 K
T= 273 K
LN (INTENSITY)
SHIFTED PLOTS---->
0
160
320
480
640
800
TIME (NSEC)

Figure 17. Ln plot of the long decay constant versus temperature for Ar/Xe=20 Torr/ 480 Torr.

Ar/Xe=20Torr/480Torr

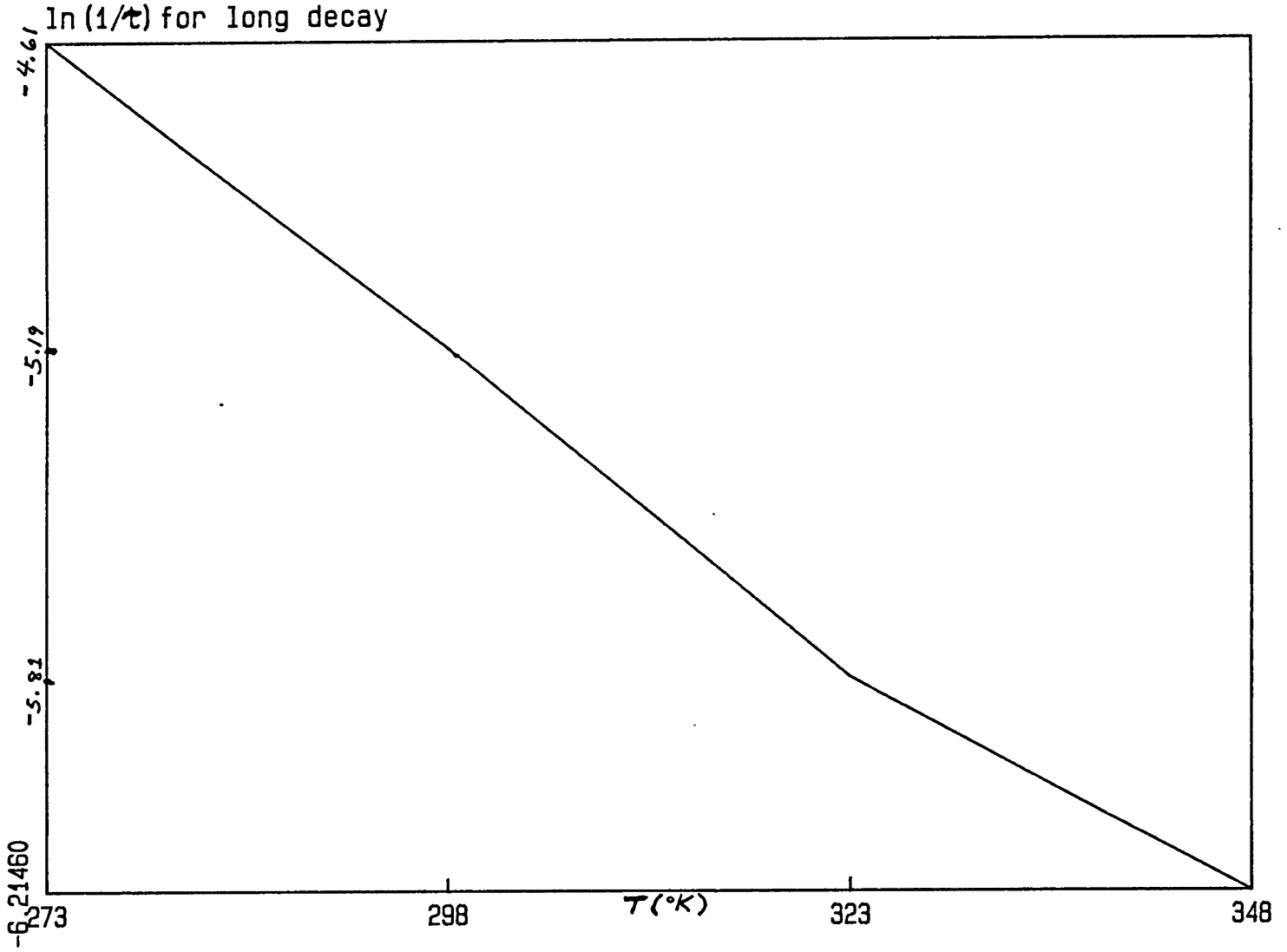

with respect to the long decay component. When Millet et al. studied the 328nm $(ArXe)^+$ emission, they reported seeing only a single component: that of the long decay. For a like gas mixture their data implies a time constant measurement of approximately 80 ns which is somewhat lower than the apparent 150 ns time constant determined in this experiment. This may be partially reconciled by considering that their data may contain an unresolved fast decay component. If one unknowingly includes this fast component in the time constant measurement, the decay appears faster than it actually is. Assuming that there is a fast component in the decay as seen in this experiment the work of Millet et al. may lack proper resolution explaining their shorter decay constant.

As stated in an earlier section, the model proposed by Millet et al. suggests only two kinetic processes: three-body collisional formation, observed in the decay or fall, and destruction by radiative decay, observed in the rise. In this experiment, temperature dependence of the long decay component seems inconsistent with that model. If the long decay component represents collisional formation, one would expect its rate to vary weakly with temperature, since collisional formation is not thermally activated [21]. However, as illustrated in figure 17, the long decay component does not exhibit "weak" temperature dependence. That is, as T increases, the decay rate decreases dramatically, implying slower molecular formation for higher temperatures. The data therefore suggests that the model proposed by Millet et al. (case (1) of Prototype Kinetic Model) is somehow incorrect.

It seems plausible that two-body collisional destruction should be an important process, considering the weak binding in heteronuclear ions. As shown in case (2) (Prototype Kinetic Model), inclusion of this process as a dominant event results in an approximate model having the long decay

component proportional to the equilibrium constant between three-body formation and two-body destruction. This equilibrium constant,equal to the formation rate divided by the destruction rate (kf/kd) should decrease with increasing temperature.This follows from the fact that two-body destruction of the molecular ion is thermally activated [22]. This picture is consistent with the observed temperature dependence. As evidenced by the plot in figure 17, the temperature dependence of the long decay component appears to be exponential. In fact, by applying the Arrhenius equation [23] kc=Cexp(-Ea/kT) to the temperature dependence of the long decay component shown in figure 17, one finds an activation energy, Ea, of approximately -.16eV. According to case (2), the long decay component is proportional to the equilibrium constant (kf/kd).If one assumes the three-body formation rate constant, kf, to be essentially constant with temperature, then kc is proportional to 1/kd. This implies that the two-body rate activation energy is roughly .16eV (-Ea), which approximates the binding energy of the $(ArXe)^+$ (IV 1/2) molecular ion.

The apparent agreement of the case (2) approximation is discredited by the evidence of preliminary data, shown in figure 18, which confirms the quadratic dependence of decay rate on xenon gas pressure reported by Millet et al.[7] . As shown earlier,the case (2) approximation results in a linear dependence of decay rate on xenon pressure.

It is apparent that our understanding of this system is far from complete at present. More extensive experimental data,hopefully,will guide us to a more accurate kinetic model.

Figure 18. Linear plot of the long decay constant versus Xe pressure for Ar fixed at 50 Torr.

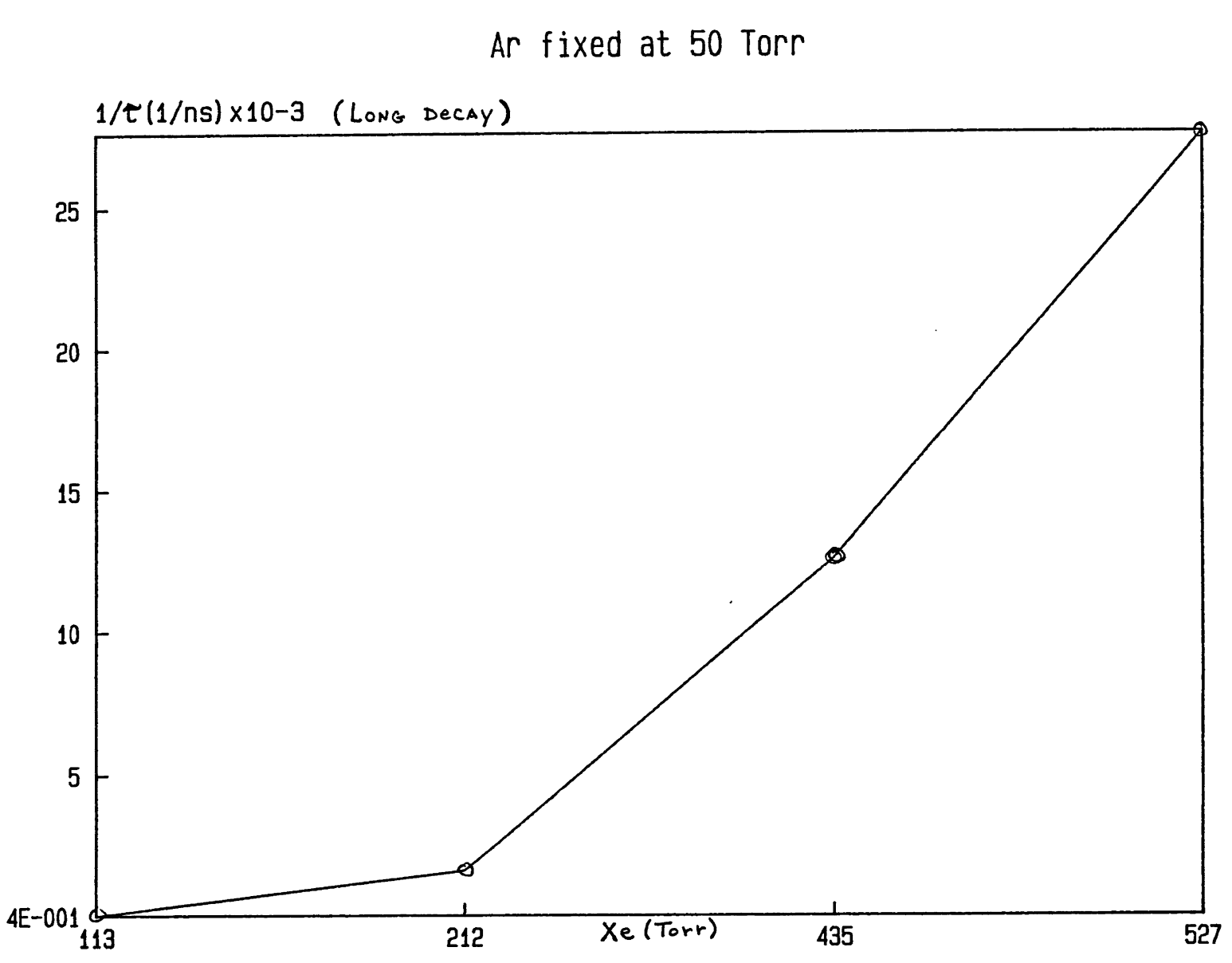
Ar fixed at 50 Torr
1/τ(1/ns) x10-3 (Long Decay)
25
20
15
10
5
4E-001
113
212
Xe (Torr)
435
527

CONCLUSIONS

The variable temperature cell that was designed, constructed and installed for the present work functioned reliably over the temperature range 248 to 348K in preliminary studies of the 328nm $(ArXe)^+$ heteronuclear ion emission.

As this thesis is only a report on preliminary work, it is impossible, at this time to make definite conclusions. However, one might say that the basic assumption of this work was shown to be valid. That is, weak binding in heteronuclear diatomic ions gives rise to strong temperature dependence in their time dependent spectra.

A direct consequence of the temperature dependence is evidence against the model proposed by Millet et al. [7] to describe this system. The temperature dependence also suggests a binding energy of approximately .18eV for the $(ArXe)^+$ (IV 1/2) molecular ion.

Two limiting cases of a kinetic model were discussed, both of which show some agreement to data, but are, nevertheless, clearly inadequate.

Due to, perhaps, better experimental conditions, a fast rise component and a fast decay component, not seen by Millet et al. was seen in this work. By further experimentation, it is hoped that added information on these fast components, plus temperature dependence, will help reveal a more accurate kinetic model.

REFERENCES

1. D. C. Lorents, Physics 82C. 19 (1976).
2. Sandia Laboratory Report SLA-73-0954, unpublished.
3. Y. Tanaka, K..Yoshino and D. E. Freeman, J. Chem. Phys. 62,4484 (1975).
4. W. Friedl, Z. Naturforsch 14a. 848 (1959); 15a. 398 (1960).
5. E. Kugler, Annalen Der Physik 14. 137 (1964).
6. B. Forestier and B. Fontaine, C.R. Acad. Sci.. Paris 286. 207 (1978).
7. P. Millet A.M. Barrie A. Birot H.Brunet H. Dijols J. Galy and Y. Salamero. J. Phys. B: At. Mol. Phys. 14. (1981) 459-472.
8. E. U. Condon and G. H. Shortley. The Theory of Atomic Spectra. Cambridge University Press (1970).
9. G. Herzberg. Molecular Spectra and Molecular Structure. Vol. I Spectra of Diatomic Molecules. Van Nostrand Reinhold Company New York (1950), pg. 378.
10. R. S. Mulliken J. Chem. Phys. 52 5170 (1970).
11. B. Schneider and J. S. Cohen. J. Chem. Phys. 61, 3240 (1974).
12. W. C. Ermler, Y. S. Lee, K. S. Pitzer and N. W. Winter, J. Chem. Phys. 69. 976 (1978).
13. Y. Tanaka, K. Yoshino and D. E. Freeman, J. Chem. Phys. 59. 5160 (1973).
14. Reference (9), p. 390.
15. Reference (9), p. 392.
16. Reference (9), p. 351.
17. C. F. Bender and N. W. Winter, Appl. Phys. Lett. 33. 533 (1978).
18. T. D. Bonifield, Time Resolved Spectroscopy of Krypton and Xenon Molecules Excited by Electron Impact and by Synchrotron Radiation. Ph.D. Thesis.

Rice University. unpublished.

19. Reference (18), p. 95.

20. R.E. Gleason, Formation and Decay of Argon and Xenon Molecules Radiating in the Vacuum Ultraviolet, M.A. Thesis, Rice University, unpublished.

21. W. G. Vincenti and C. H. Kruger, Introduction to Physical Gas Dynamics, John Wiley and Sons, Inc., New York (1965), pg. 225.

22. Reference (21), p. 223.

23. Reference (21), p. 214.